A unified charge-based model for SOI MOSFETs applicable from intrinsic to heavily doped channel*

Zhang Jian(张 健)[a], He Jin(何 进)[a)b)†], Zhou Xing-Ye(周幸叶)[a], Zhang Li-Ning(张立宁)[a], Ma Yu-Tao(马玉涛)[b], Chen Qin(陈 沁)[b], Zhang Xu-Kai(张勖凯)[b], Yang Zhang(杨 张)[b], Wang Rui-Fei(王睿斐)[b], HanYu(韩 雨)[b], and Chan Mansun(陈文新)[c]

[a] *Tera-Scale Research Centre (TSRC), School of Electronics Engineering and Computer Science (EECS), Peking University, Beijing* 100871, *China*

[b] *Peking University Shenzhen System on Chip (SOC) Key Laboratory, PKU–HKUST Shenzhen–Hongkong Institution, W303, West Tower, IER Bldg, Hi-Tech Industrial Park South, Shenzhen* 518057, *China*

[c] *Department of Electronics and Computer Engineering (ECE), Hong Kong University of Science and Technology, Kowloon, Clearwater Bay, Hong Kong, China*

(Received 26 July 2011; revised manuscript received 26 October 2011)

A unified charge-based model for fully depleted silicon-on-insulator (SOI) metal–oxide semiconductor field-effect transistors (MOSFETs) is presented. The proposed model is accurate and applicable from intrinsic to heavily doped channels with various structure parameters. The framework starts from the one-dimensional Poisson–Boltzmann equation, and based on the full depletion approximation, an accurate inversion charge density equation is obtained. With the inversion charge density solution, the unified drain current expression is derived, and a unified terminal charge and intrinsic capacitance model is also derived in the quasi-static case. The validity and accuracy of the presented analytic model is proved by numerical simulations.

Keywords: charge-based model, silicon-on-insulator metal–oxide semiconductor field-effect transistors, compact model, double gate

PACS: 73.40.Ty, 73.40.Qv, 61.44.Br **DOI:** 10.1088/1674-1056/21/4/047303

1. Introduction

With continuous scaling down, traditional bulk metal–oxide semiconductor field-effect transistors (MOSFETs) suffer from severe short channel effects and gate tunneling,[1] and silicon-on-insulator (SOI) MOSFETs have become a mainstream technology for high-performance and low-power applications due to the advantages of the unique SOI structure, such as good isolation and latch-up free operation.[1−4] In addition, the fully depleted device has a high drive current, suppression of the floating body effect, and low junction tunneling current.[2−4] In particular for nanoscale devices and integrated circuit (IC) design, ultra-thin-body (UTB) SOI MOSFETs with a fully depleted body show potentially superior scalability relative to their partially depleted and bulk complementary metal–oxide semiconductor (CMOS) counterparts.[4−7]

In order to realize these advantages for integrated circuit design, there has been much research done on compact modeling for fully depleted SOI MOSFETs.[8−24] These mainstream models are mainly surface potential-based,[8−13] charge-based,[14−20] threshold voltage-based,[21] and others.[22−24] The traditional threshold-voltage-based models have limitations in rising radio frequency (RF) circuit design applications because of their discontinuities in derivatives, asymmetries, etc.[12,22] The potential-based models which express the charge and current in terms of the surface potential, and the charge-based models that formulate the terminal charges and drain current with the inversion charge density, have potential in analog and RF CMOS simu-

*Project supported by the National Natural Science Foundation of China (Grant No. 60876027), the State Key Program of the National Natural Science Foundation of China (Grant No. 61036004), the Shenzhen Science and Technology Foundation, China (Grant No. CXB201005250031A), the Fundamental Research Project of Shenzhen Science and Technology Foundation, China (Grant No. JC201005280670A), and the International Collaboration Project of Shenzhen Science & Technology Foundation, China (Grant No. ZYA2010006030006A).

†Corresponding author. E-mail: frankhe@pku.edu.cn

© 2012 Chinese Physical Society and IOP Publishing Ltd

lation applications.[8,9,14−17] A charge-based model for fully depleted SOI MOSFETs has been presented earlier, and it describes the different operating regimes, respectively.[15−17] In recent studies, a unified charge control model was derived for fully depleted structures for the first time.[18] However, this model deals with highly doped and undoped devices with different expressions, and the variation in the buried oxide thickness is also neglected by assuming it to be equal to the front-gate oxide thickness.[18,19] However, since the thin buried oxide may induce the loss of speed and thereby complicate the technology, the thick-buried-oxide device may be a better design.[25] Thus a unified model considering various structure parameter variations is still lacking for circuit design applications with fully depleted devices.

In this paper, a unified charge-based model for fully depleted SOI MOSFETs is presented, which is accurate and applicable to intrinsic and heavily doped devices with various structure parameter variations. Starting from the one-dimensional (1D) Poisson–Boltzmann equation, an accurate inversion charge density equation is obtained based on the full depletion approximation. With the inversion charge density solution, the unified drain current expression is derived, which is physically continuous between the subthreshold and strong inversion regions. The unified terminal charge and intrinsic capacitance model is also derived in the quasi-static case as an explicit function of the inversion charge solution at both the source and drain ends. The validity and accuracy of the presented analytic model are proved by numerical simulations. In the absence of quantum mechanical effects (QME) and poly-silicon effects (PSE), the large application scope of various structure parameters not only proves the practicability of the long-channel model as the basis for the development of improved models for actual devices, as well as for the extraction of device parameters, but also gives an instructive reference to the compact modeling of symmetric and independent double-gate MOSFETs, which is based on the same oxide–silicon–oxide structure as SOI MOSFETs.

2. Model development

The analysed device is a typical four-terminal n-channel SOI MOSFET, as illustrated in Fig. 1, where the x axis is perpendicular to the surface and the y axis is along the channel in the corresponding coordinates. The doping concentration of the substrate is assumed to be high enough and the voltage drop on the substrate is neglected.

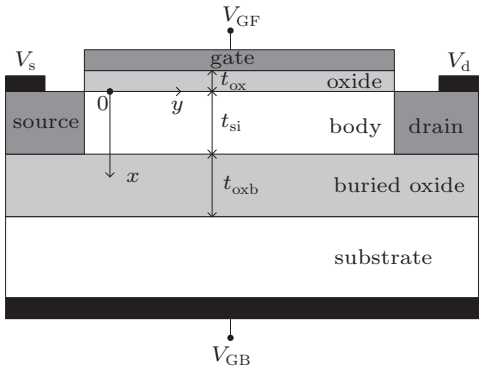


Fig. 1. Schematic diagram of the SOI MOSFET.

2.1. Unified drain current model

In the SOI MOSFET, the long-channel approximation is accurate as long as the channel length L is much larger than the λ introduced in Ref. [3] and expressed as

$$\lambda = \sqrt{\frac{\varepsilon_{si}}{\varepsilon_{ox}} t_{ox} t_{si}}, \tag{1}$$

where ε_{si} and ε_{ox} are silicon permittivity and oxide permittivity, respectively, and t_{si} and t_{ox} represent the thicknesses of the body silicon film and front-gate oxide. Under the gradual-channel approximation, considering both fixed charge and electron, the 1D Poisson–Boltzmann's equation is written as

$$\frac{\mathrm{d}^2\phi}{\mathrm{d}x^2} = \frac{qN_A}{\varepsilon_{si}} \Big[1 + \exp\Big(\frac{\phi - 2\phi_F - V_{ch}}{V_t}\Big)\Big], \tag{2}$$

where ϕ denotes the electrostatic potential, x is the direction perpendicular to the channel, q is the magnitude of electron charge and N_A is the doping concentration of the body silicon film. ϕ_F and V_{ch} are Fermi potential ($\phi_F = V_t \ln(N_A/n_i)$) and quasi-Fermi potential, respectively, V_t represents the thermal voltage ($V_t = kT/q$), k is Boltzmann's constant, and T is absolute temperature.

With Gauss's law, the electric fields at the body silicon film front and back surfaces are expressed as

$$\varepsilon_{si}(E_s - E_0) = Q_{dep} + Q_{inv}, \tag{3a}$$

$$\varepsilon_{si} E_s = C_{ox}(V_{GF} - \phi_s), \tag{3b}$$

$$\varepsilon_{si} E_0 = C_{oxb}(\phi_0 - V_{GB}), \tag{3c}$$

where E_s and E_0 are the front interface and back interface electric fields perpendicular to the surface, respectively. Q_{inv} and Q_{dep} denote the inversion charge and depletion charge densities, respectively. ϕ_s and ϕ_0 are the electrostatic potential at the front and back interface of the silicon body, respectively. C_{ox} and C_{oxb} represent the gate oxide and buried oxide capacitances per unit area ($C_{ox(b)} = \varepsilon_{ox}/t_{ox(b)}$), respectively, and t_{oxb} is the thickness of the buried oxide. V_{GF} and

$V_{\rm GB}$ are the front-gate voltage and substrate voltage, respectively.

The relationship between the potentials at the interfaces between the silicon and oxides in the depletion approximation is given as[10,26−28]

$$\phi_{\rm s}-\phi_0=\frac{qN_{\rm A}t_{\rm si}^2}{2\varepsilon_{\rm si}}+E_0t_{\rm si}\triangleq V_{\rm B}+E_0t_{\rm si}. \tag{4}$$

Integrating the Poisson–Boltzmann equation yields[10,12]

$$\begin{aligned}\varepsilon_{\rm si}^2(E_{\rm s}^2-E_0^2)=&2qN_{\rm A}\varepsilon_{si}\Big\{\Big(\phi_{\rm s}-\phi_0\Big)\\&+V_{\rm t}\exp\Big(\frac{\phi_{\rm s}-2\phi_{\rm F}-V_{\rm ch}}{V_{\rm t}}\Big)\\&\times\Big[1-\exp\Big(\frac{\phi_0-\phi_{\rm s}}{V_{\rm t}}\Big)\Big]\Big\}.\end{aligned} \tag{5}$$

Substituting Eq. (4) into Eq. (5), and combining it with Eq. (3a), yields

$$\begin{aligned}Q^2+2\varepsilon_{\rm si}E_0Q=&Q_{\rm dep}^2+2\varepsilon_{\rm si}E_0Q_{\rm dep}\\&+2Q_{\rm dep}C_{\rm si}V_{\rm t}\exp\Big(\frac{\phi_{\rm s}-2\phi_{\rm F}-V_{\rm ch}}{V_{\rm t}}\Big),\end{aligned} \tag{6}$$

where Q is the total charge and $C_{\rm si}$ is the body silicon capacitance per unit area ($C_{\rm si}=\varepsilon_{\rm si}/t_{\rm si}$). For the fully depleted body silicon film, $Q_{\rm dep}=qN_{\rm A}t_{\rm si}$, and for simplification, let $\exp[(\phi_0-\phi_{\rm s})/V_{\rm t}]\approx 0$, approximately.

The charge terms and the voltage terms in Eq. (6) are normalized by $q_0=(C_{\rm ox}+C_1)V_{\rm t}$ and $V_{\rm t}$, respectively. The lowercase letters represent the corresponding normalized terms. And then simplifying Eq. (6) yields

$$q_{\rm inv}+Hq_{\rm inv}^2=\frac{C_{\rm si}q_{\rm dep}}{(C_{\rm ox}+C_1)q_1}\exp(\phi_{\rm s}-2\phi_{\rm f}-v_{\rm ch}), \tag{7}$$

where

$$\begin{aligned}C_1&=\frac{C_{\rm oxb}C_{\rm si}}{C_{\rm oxb}+C_{\rm si}},\\q_1&=\frac{1}{q_0}\frac{C_{\rm ox}}{C_{\rm ox}+C_1}\Big[\frac{Q_{\rm dep}}{\beta}+C_1(V_{\rm GF}-V_{\rm B}-V_{\rm GB})\Big],\\H&=\frac{C_{\rm ox}-C_1}{C_{\rm ox}+C_1}\frac{1}{2q_1},\end{aligned}$$

with $\beta=1-\exp(-2v_{\rm b})$ for the accurate modeling from intrinsic to heavy channel doping concentrations.[14,18,19,29]

Calculating the logarithm in Eq. (7) and eliminating $\varphi_{\rm s}$ from Eqs. (3) and (4), we have

$$\begin{aligned}&q_{\rm inv}+\ln q_{\rm inv}+\ln(1+Hq_{\rm inv})\\&=v_1-q_{\rm dep}-2\phi_{\rm f}-v_{\rm ch}+\ln\Big[\frac{C_{\rm si}q_{\rm dep}}{(C_{\rm ox}+C_1)q_1}\Big],\end{aligned} \tag{8}$$

where

$$v_1=\frac{1}{V_{\rm t}}\frac{C_{\rm ox}V_{\rm GF}+C_1(V_{\rm B}+V_{\rm GB})}{C_{\rm ox}+C_1}.$$

This inversion charge density equation (8) contains all the structure parameters such as $N_{\rm A}$, $t_{\rm si}$, $t_{\rm ox}$, and $t_{\rm oxb}$, and the controllable variables $V_{\rm GF}$, $V_{\rm GB}$, and $V_{\rm ch}$. Thus the proposed model can effectively handle all these parameter variations.

The DC drain current of SOI MOSFETs is expressed as[30]

$$I_{\rm ds}=\mu\frac{W}{L}\int_0^{V_{\rm ds}}Q_{\rm inv}\,{\rm d}V_{\rm ch}\triangleq\mu\frac{W}{L}(C_{\rm ox}+C_1)V_{\rm t}^2\cdot i_{\rm ds}, \tag{9}$$

where $I_{\rm ds}$ is the drain current and $i_{\rm ds}$ is the normalized drain current, $V_{\rm ds}$ is the voltage between the drain and the source, μ is the effective electron mobility, and W and L are the channel width and channel length, respectively.

From Eq. (8), it is easily obtained that

$$\frac{{\rm d}v_{\rm ch}}{{\rm d}q_{\rm inv}}=-\Big(1+\frac{1}{q_{\rm inv}}+\frac{H}{1+Hq_{\rm inv}}\Big). \tag{10}$$

So the drain current equation (9) is derived as

$$i_{\rm ds}=\int_0^{V_{\rm ds}}q_{\rm inv}\,{\rm d}v_{\rm ch}=F(q_{\rm inv}3)|_{q_{\rm s}}^{q_{\rm d}} \tag{11a}$$

with

$$F(q_{\rm inv})=-\Big[\frac{q_{\rm inv}^2}{2}+2q_{\rm inv}-\frac{1}{H}\ln(1+Hq_{\rm inv})\Big], \tag{11b}$$

where $q_{\rm d}$ and $q_{\rm s}$ are the normalized inversion charge densities at the source ($V_{\rm ch}=V_{\rm s}$) and drain ($V_{\rm ch}=V_{\rm d}$) ends, which are calculated from the inversion charge density equation (8).

In particular, for a symmetric DG MOSFET, half of it is regarded as a special SOI structure with infinite buried oxide thickness. So in the above derivation, $C_{\rm oxb}$ is zero and the inversion charge density equation (8) is simplified as

$$\begin{aligned}q_{\rm inv}+\ln q_{\rm inv}+\ln(1+Hq_{\rm inv})=&v_{\rm gf}-q_{\rm dep}-2\phi_{\rm f}-v_{\rm ch}\\&+\ln\Big[\frac{\beta C_{\rm si}}{C_{\rm ox}}\Big],\end{aligned} \tag{12}$$

with $H=\beta/2q_{\rm dep}$. The drain current expression also reduces to the same form as Eq. (11), but with a simpler coefficient H.[18,19,31]

2.2. Unified terminal charge and intrinsic capacitance model

The charges are related by the neutrality condition

$$Q_{\rm GF}+Q_{\rm GB}+Q_{\rm N}+Q_{\rm B}=0, \tag{13}$$

where $Q_{\rm GF}$, $Q_{\rm GB}$, $Q_{\rm N}$, and $Q_{\rm B}$ are the front-gate, back-gate, inversion charges, and depletion charge, respectively. Here, the interface-state charge is neglected, and four principal charges are described as

$$Q_{\rm GF} = W\int_0^L C_{\rm ox}(V_{\rm GF}-\phi_{\rm s})\,{\rm d}y, \tag{14a}$$

$$Q_{\rm GB} = W\int_0^L C_{\rm ox}(V_{\rm GB}-\phi_{0})\,{\rm d}y, \tag{14b}$$

$$Q_{\rm N} = -Wq_0\int_0^L q_{\rm inv}\,{\rm d}y, \tag{14c}$$

$$Q_{\rm B} = -Wq_0\int_0^L q_{\rm dep}\,{\rm d}y. \tag{14d}$$

For the fully depleted body, the body charge $q_{\rm dep}$ is a constant, thus

$$Q_{\rm B} = -WLq_0q_{\rm dep}. \tag{15}$$

The channel inversion charge is

$$Q_{\rm N} = -Wq_0\int_0^L q_{\rm inv}\,{\rm d}y = -\frac{WLq_0}{i_{\rm ds}}\int_0^L q_{\rm inv}^2\,{\rm d}v_{\rm ch}. \tag{16a}$$

Combining Eq. (16a) with Eq. (10) and performing the above integral, we have

$$Q_{\rm N} = WLq_0\frac{M(q_{\rm inv})|_{q_{\rm s}}^{q_{\rm d}}}{i_{\rm ds}}, \tag{16b}$$

$$M(q_{\rm inv}) = \frac{q_{\rm inv}^3}{3}+q_{\rm inv}^2-\frac{q_{\rm inv}}{H} + \frac{1}{H^2}\ln[1+Hq_{\rm inv}]. \tag{16c}$$

From Poisson–Boltzmann's equation (1) and Gauss's law (2), equation (14b) is derived as

$$Q_{\rm GB} = -Wq_0\int_0^L\Big(q_2-\frac{C_1}{C_{\rm ox}+C_1}q_{\rm dep} - \frac{C_1}{C_{\rm ox}+C_1}q_{\rm inv}\Big)\,{\rm d}y, \tag{17a}$$

where

$$q_2 = \frac{1}{q_0}\frac{C_1C_{\rm ox}(V_{\rm GF}-V_{\rm B}-V_{\rm GB})}{(C_{\rm ox}+C_1)}.$$

Performing the above integration, we thus have

$$Q_{\rm GB} = -WLq_0\Big(q_2-\frac{C_1}{C_{\rm ox}+C_1}q_{\rm dep} - \frac{C_1}{C_{\rm ox}+C_1}\frac{M(q_{\rm inv})|_{q_{\rm s}}^{q_{\rm d}}}{i_{\rm ds}}\Big). \tag{17b}$$

Once three charges are obtained, the other charge is also obtained from the neutrality condition (13) as

$$Q_{\rm GF} = -(Q_{\rm GB}+Q_{\rm N}+Q_{\rm B}), \tag{18a}$$

yielding

$$Q_{\rm GF} = WLq_0\Big(q_2+\frac{C_{\rm ox}}{C_{\rm ox}+C_1}q_{\rm dep} + \frac{C_{\rm ox}}{C_{\rm ox}+C_1}\frac{M(q_{\rm inv})|_{q_{\rm s}}^{q_{\rm d}}}{i_{\rm ds}}\Big). \tag{18b}$$

The channel inversion charge $Q_{\rm N}$ is partitioned between the drain and source according to Ward and Dutton's charge partition model,[32] and the drain terminal charge is expressed as

$$Q_{\rm D} = -Wq_0\int_0^L\frac{y}{L}q_{\rm inv}\,{\rm d}y. \tag{19}$$

Combining the current continuity with the drain current expression (11) in the quasi-static case, the relationship between y and $q_{\rm inv}$ is derived as

$$y = \frac{L}{i_{\rm ds}}\Big\{2(q_{\rm s}-q_{\rm inv})+\frac{(q_{\rm s}^2-q_{\rm inv}^2)}{2} + \frac{1}{H}\ln\Big[\frac{1+H\cdot q_{\rm inv}}{1+H\cdot q_{\rm s}}\Big]\Big\}. \tag{20}$$

After complicated calculations, the drain terminal charge is finally obtained as

$$Q_{\rm D} = -WLq_0\frac{[M(q_{\rm inv})F(q_{\rm s})+N(q_{\rm inv})]|_{q_{\rm s}}^{q_{\rm d}}}{i_{\rm ds}^2}, \tag{21a}$$

$$N(q_{\rm inv}) = \Big[-\frac{q_{\rm inv}^5}{10}-\frac{3}{4}q_{\rm inv}^4-\frac{2q_{\rm inv}^3}{3}\Big]+\frac{1}{H}\Big[q_{\rm inv}^2\ln(1+Hq_{\rm inv})+\frac{q_{\rm inv}^2}{2}+\frac{q_{\rm inv}^3}{3}\ln(1+Hq_{\rm inv})+\frac{q_{\rm inv}^3}{18}\Big] + \frac{1}{H^2}\Big[-\frac{q_{\rm inv}^2}{12}-q_{\rm inv}\ln(1+Hq_{\rm inv})\Big]+\frac{1}{H^3}\Big[\frac{1}{6}q_{\rm inv}^+\ln(1+Hq_{\rm inv})\Big]+\frac{1}{H^4}\Big[-\frac{1}{6}\ln(1+Hq_{\rm inv})\Big]. \tag{21b}$$

And the source terminal charge is obtained similarly as

$$Q_{\rm S} = Q_{\rm N}-Q_{\rm D} = -WLq_0\frac{[M(q_{\rm inv})F(q_{\rm d})+N(q_{\rm inv})]|_{q_{\rm d}}^{q_{\rm s}}}{i_{\rm ds}^2}. \tag{22}$$

As a four-terminal device, SOI MOSFETs have 16 capacitances. Among them, only nine capacitances are independent.[15,33,34] These capacitances are defined as

$$C_{ij} = \begin{cases} -\dfrac{\partial Q_i}{\partial V_j},\ i\neq j, \\ \dfrac{\partial Q_i}{\partial V_j},\ i=j, \end{cases} \quad i,j = {\rm GF,GB,S,D}. \tag{23}$$

With the terminal charge expressions (17), (18), (21), and (22), the above partial derivatives and the capacitance matrix are easily obtained for fully depleted SOI MOSFETs. All the capacitances are expressed by explicit functions of the inversion charge density at the source and drain ends.

3. Results and discussion

To verify the proposed analytical model, a long-channel SOI MOSFET with constant mobility is designed for the two-dimensional numerical simulation.[35] A doping concentration of 1×10^{18} cm^{-3} for the substrate silicon film, constant electron mobility of 350 cm^2/V·s, and metal gate with mid-gap work-function are used. The width of the channel is 1 μm. And to avoid the short channel effects and prove the validity of the long channel theory, a channel length of 5 μm is used.

Figure 2 shows the inversion charge densities in the silicon film each as a function of gate voltage under $V_{ds} = 0$ for different channel doping concentrations. Figure 3 exhibits the drain currents predicted by the unified current model and the numerical simulation results, each as a function of V_{gs} for some different values of V_{ds}. Good agreement between the proposed model and the numerical simulation are observed from weak inversion through moderate inversion to the strong inversion regions.

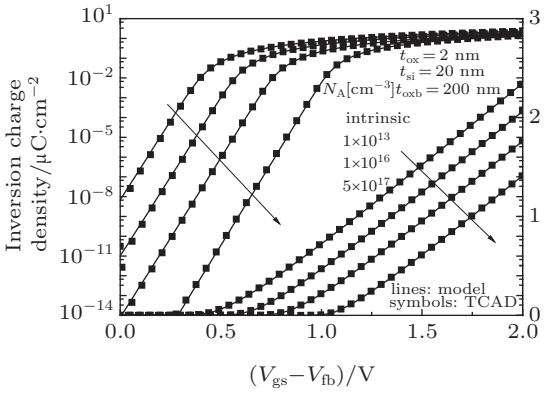


Fig. 2. Comparisons of inversion charge density between the model predicted results (lines) and the numerical results (symbols), each as a function of gate voltage for the cases of four different doping levels.

In the absence of QME and PSE, the application scope of various structure parameters for the model is widely verified. Figure 4 shows the drain currents calculated from the model, compared with the numerical results for different channel doping levels from intrinsic to heavily doped conditions. The unified current model predictions accord well with the simulations at up to a 5×10^{17} cm^{-3} body doping.

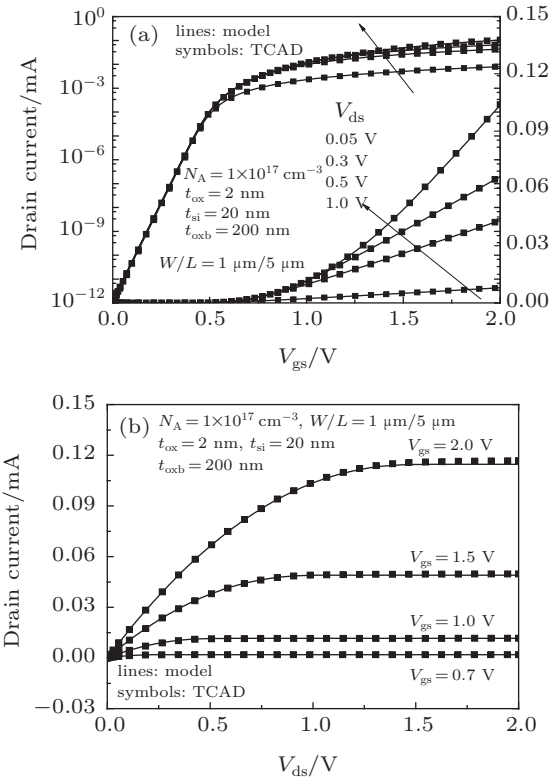


Fig. 3. Drain currents calculated from the unified current model and numerical simulation: (a) transfer characteristics and (b) output characteristics.

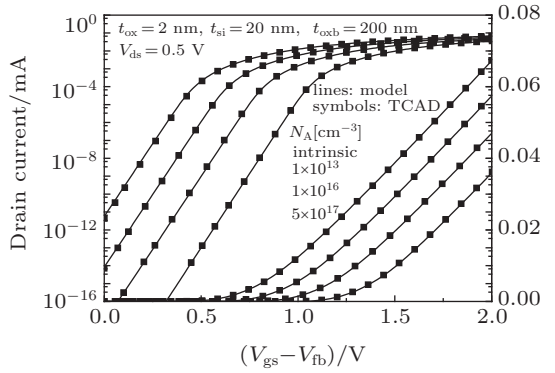


Fig. 4. Transfer characteristics of devices with different doping levels, from the intrinsic to the heavily doped condition. The lines represent the unified current model predicted results, and the symbols denote the results from numerical simulations.

Figures 5–8 display the drain currents with different structure parameters, such as silicon film thickness, gate oxide thickness, buried oxide thickness, and back gate bias. Figure 5 shows the influence of silicon thickness on drain current for both the intrinsic and heavily doped channels. The volume inversion is observed for a lightly doped device, where the subthreshold leakage is linearly proportional to t_{si}. On the other hand, for the heavily doped device, the drain current is inversely proportional to t_{si} because of the

increase in body fixed charge.[36,37] This unique characteristic is accurately accounted for with the unified current model. Figures 6–8 also show accurate modeling of the devices with different oxide thicknesses and back gate biases for both intrinsic and heavily doped silicon films. These results show the ability to predict the electric field at the interface, which is quite important for predicting the characteristics of the oxide–silicon–oxide structure, such as the suppression of short-channel-effect (SCE) and mobility degradation.[25] The large application scopes of the various structure parameters not only prove the validity and the practicability of the proposed model, but also give a reference to the compact modeling of symmetric and independent double gate MOSFETs.

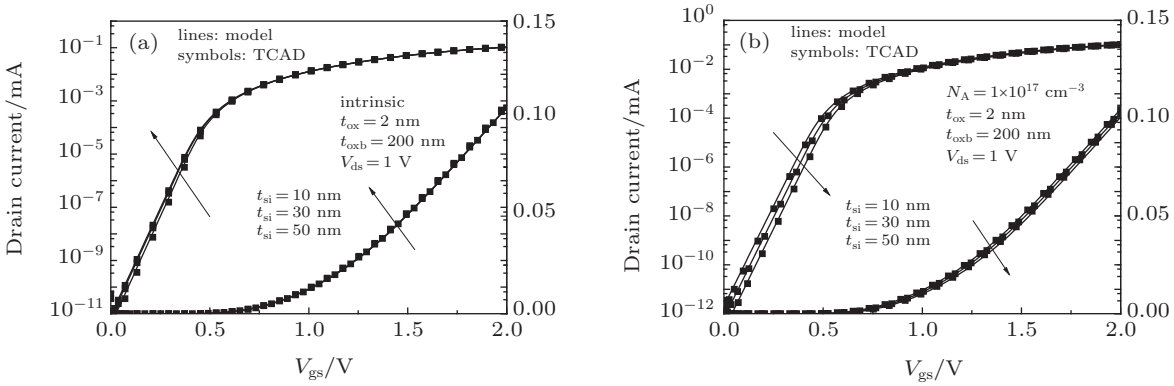


Fig. 5. Transfer characteristics of devices with different silicon film thicknesses, obtained from the unified drain current model (lines) and numerical simulation (symbols). (a) Devices with intrinsic channels; (b) devices with heavily doped channels.

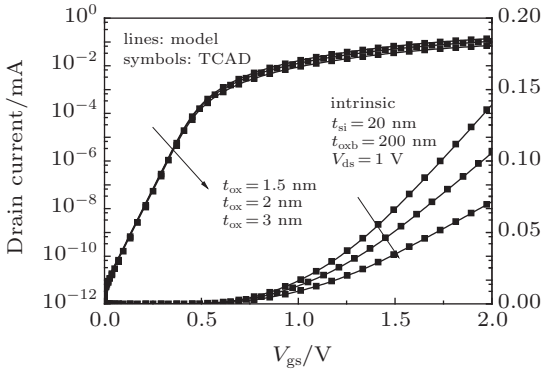


Fig.6. Transfer characteristics of devices with intrinsic channels and different gate oxide thicknesses, obtained from the unified drain current model (lines) and numerical simulation (symbols).

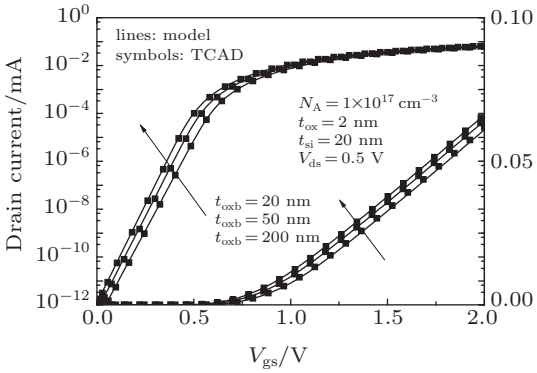


Fig.7. Transfer characteristics of devices with heavily doped channels and different buried oxide thicknesses, obtained from the unified drain current model (lines) and numerical simulation (symbols).

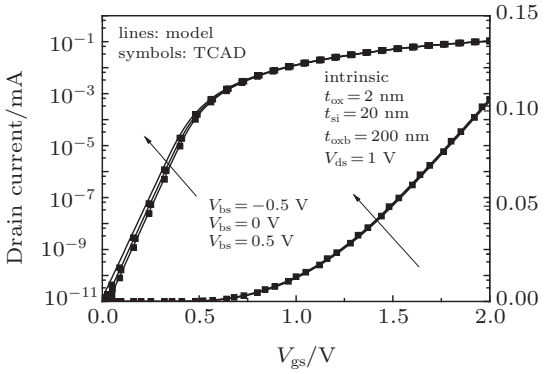


Fig. 8. Transfer characteristics of devices with intrinsic channels and different back-gate biases, obtained from the unified drain current model (lines) and numerical simulation (symbols).

Figure 9 indicates the normalized capacitances calculated from the unified capacitance model and their comparisons with the numerical simulation results. Figure 9(a) shows the capacitances versus gate voltage. The trans-capacitances (C_{gd}, C_{dg}), (C_{gs}, C_{sg}), and (C_{sd}, C_{ds}) are all different, conforming with the nonreciprocal characteristics.[33,34] Figure 9(b) displays the capacitances versus drain voltage. The results from the proposed model and the TCAD results are shown to be in good agreement in Figs. 9(a) and 9(b). The symmetry of the trans-capacitances, e.g. $C_{gs} = C_{gd}$ when $V_{ds} = 0$, is also ac-

curately predicted by the proposed capacitance model.

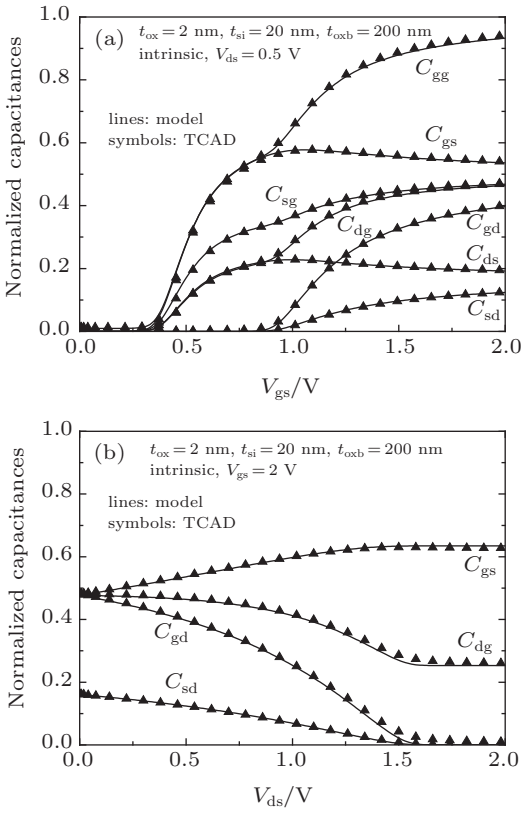


Fig. 9. Normalized independent capacitances of a fully depleted SOI MOSFET with intrinsic body, obtained from the unified model (lines) and numerical simulation (symbols). (a) Capacitances versus gate voltage, and (b) capacitances versus drain voltage.

4. Conclusions

In this paper, a unified charge-based model for fully depleted SOI MOSFETs is presented. An accurate inversion charge density equation is obtained based on the full depletion approximation. With this inversion charge density solution, the unified drain current expression is derived. The quasi-static terminal charge and intrinsic capacitance are also derived. This work gives an accurate compact model for the device with both intrinsic and heavily doped channels. Extensive verification with numerical simulations for the various structure parameters proves the accuracy and the practicability of the proposed model. For the devices with the same oxide–silicon–oxide structure, such as symmetric and independent double gate MOSFETs, the presented result also gives an instructive reference for compact modeling.

References

[1] Frank D J, Dennard R H, Nowak E and Solomon P M 2001 *Proc. IEEE* **89** 259
[2] Colinge J P *Proceedings of the 34th European Solid-State Device Research Conference* September 21–23, 2004 Leuven, Belgium, p. 45
[3] Yang R H, Ourmazd A and Lee K F 1992 *IEEE Trans. Electron Dev.* **39** 1704
[4] Trivedi V P and Fossum J G 2003 *IEEE Trans. Electron Dev.* **50** 2095
[5] Suzuki E, Ishii K, Kanemaru S and Maeda T 2000 *IEEE Tran. Electron Dev.* **47** 354
[6] Doris B, Ieong M and Kanarsky T *International Electron Devices Meeting Technical Digest* December 8–11, 2002 San Francisco, USA, p. 267
[7] Fossum J G 2007 *Solid-State Electronics* **51** 188
[8] Norio Sadachika, Daisuke Kitamaru and Yasuhito 2006 *IEEE Trans. Electron Dev.* **53** 2017
[9] Wu W, Yao W and Gildenblat G 2008 *IEEE Trans. Electron Dev.* **55** 3295
[10] Sleight J W and Rafael Rios 1998 *IEEE Trans. Electron Dev.* **45** 821
[11] Ortiz-Conde A, Herrera R and Schmidt P E 1992 *Solid-State Electronics* **35** 1291
[12] Zhou X, Chandrasekaran K and Chiah S B *Technical Proceedings of the 2006 Nanotechnology Conference and Trade Show* May 8–11, 2006 Boston, USA, p. 652
[13] Niu G F, Chen R M M and Ruan C 1996 *IEEE Trans. Electron Dev.* **43** 2034
[14] Roy A S, Sallese J M and Enz C C 2006 *Solid State Electron* **50** 687
[15] Lim H K and Fossum J G 1985 *J. Solid State Circuits* **20** 366
[16] Veeraraghavan S and Fossum J G 1988 *IEEE Trans. Electron Dev.* **35** 1866
[17] Yeh P C and Fossum J G 1995 *IEEE Trans. Electron Dev.* **42** 1605
[18] Moldovan O, Cerdeira A and Jiménez D 2007 *Solid-State Electronics* **51** 655
[19] Moldovan O, Chaves F A and Jiménez D 2008 *Solid-State Electronics* **52** 1867
[20] Liu F, He J and Zhang L 2008 *IEEE Trans. Electron Dev.* **55** 2187
[21] Fung S K H, Su P and Hu C *Proceedings of 5th Conference on Modeling and Simulation of Microsystems* April 2002 Puerto Rico, USA, p. 690
[22] He J, Chan M S and Zhang G G 2006 *Semicond. Sci. Technol.* **21** 261
[23] Liu F, He J and Ma Y F 2008 *IEEE Trans. Electron Dev.* **55** 816
[24] He J, Bian W and Tao Y J 2007 *IEEE Trans. Electron Dev.* **54** 1478
[25] Trivedi V P and Fossum J G Jan 2005 *IEEE Electron Dev. Lett.* **26** 26
[26] Worley E R 1980 *Solid-State Electron* **23** 1107
[27] Lim H and Fossum J G 1983 *IEEE Trans. Electron Dev.* **30** 1244
[28] Zhang J, He J and Zhang L N 2007 *IEEE International Conference on Electron Devices and Solid-State Circuits* December 20–22, 2007 Tai'an, China p. 569
[29] Sallese J M, Krummenacher F and Prégaldiny F 2005 *Solid-State Electronics* **49** 485
[30] Pao H C and Sah C T 1966 *Solid-State Electron*ics **9** 927

[31] Francis P, Terao A and Flandre D 1995 *Solid-State Electronics* **38** 171

[32] Ward D and Dutton R 1978 *IEEE J. Solid State Circuits* **13** 703

[33] Lim H K and Fossum J G 1984 *IEEE Trans. Electron Dev.* **31** 1983

[34] Liu F L, Zhang J and He F J 2009 *Solid-State Electronics* **53** 49

[35] Synopsys 2005 *Sentaurus Device User's Manual* p. 1

[36] Balestra F, Cristoloveanu S and Benachir M 1987 *IEEE Electron Dev. Lett.* **8** 410

[37] Trivedi V P, Fossum J G and Zhang W Jan 2007 *Solid-State Electronics* **51** 170